JOURNAL OF MATERIALS SCIENCE 19 (1984) 3908–3924

The influence of temperature cycling on the creep properties of Nickel 201 and Inconel 600 in combustion gas

J. K. SOLBERG*, H. THON
Central Institute for Industrial Research, Blindern, Oslo 3, Norway

The effect of temperature cycling on the creep behaviour of Nickel 201 and Inconel 600 in combustion gas has been studied. Specimens were tested both at constant temperature, 900° C, and at 900° C interrupted by temperarature drops down to ~ 510° C. The creep straining has been analysed with respect to a weighted time parameter which includes the creep contribution during the lower temperatures of each cycle. With respect to this compensated time parameter, the temperature variations were generally observed to result in a strong acceleration in creep. The effect seemed to increase with increasing frequency of temperature drops, increasing grain size and decreasing stress. Thus, at low stress levels, large-grained specimens of both alloys experienced an acceleration even in *absolute* creep rate upon cycling. The grain size dependency indicates that the destructive effect of the cycles is caused by crack formation. Surface cracking associated with grain boundary oxidation seemed to be the dominant cracking mode. It is suggested that, during creep in oxidizing environments, repeated periods of cooling might strongly accelerate the growth of surface creep cracks due to the difference in thermal expansion between metals and oxides. This difference causes high tensile stresses to arise in the metal in front of the grain boundary oxides, and the stresses are assumed to be high enough to nucleate microcracks along the boundary.

1. Introduction

Creep test data obtained under stationary conditions are frequently used as design data for applications where materials are subjected to variable conditions like non-steady stress or temperature. An example of such applications is the turbine wheel in a gas turbine. The creep properties of the turbine blades are usually estimated on the basis of creep and stress rupture tests performed at constant temperature. However, the service conditions for gas turbines include periods of heating and cooling associated with start and stop and without any change in the output. In using stationary creep data the possible effect of such temperature variations is not accounted for when the length of turbine life is estimated.

The work presented in this paper is an integral part of a comprehensive research programme recently started at the Central Institute for Industrial Research, Oslo, on degradation of high temperature alloys due to creep, corrosion and thermal cycling. The programme includes advanced turbine blade alloys as well as simpler alloys like Nickel 201 and Inconel 600. The creep properties in combustion gas of the two latter alloys were the topics of a recent paper by the present authors [1]. In this work the creep properties of the same two alloys are analysed under variable temperature conditions in combustion gas. A corresponding test programme will later be carried out for the advanced turbine alloys, and the results from these experiments will be the subject of subsequent papers.

*Present address: University of Trondheim, The Norwegian Institute of Technology, Division of Physical Metallurgy, N-7034 Trondheim – NTH, Norway.

0022–2461/84 $03.00 + .12

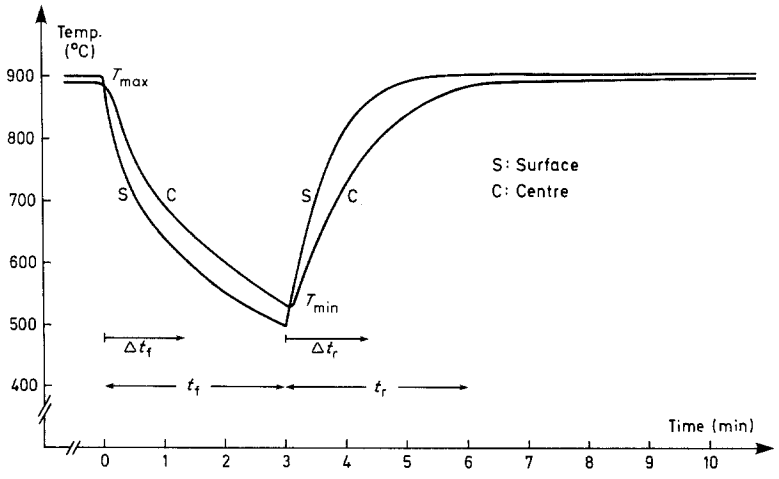

Figure 1 Typical temperature cycle during cyclic creep, recorded after 700 h test time.

2. Experimental details

2.1. Equipment

The experimental equipment consisted of a creep furnace which was connected to an oil combustion rig. Light fuel oil was burnt with an air excess of 10%. The oil had impurity additions of 2.5% sulphur, 50 p.p.m. sodium and 50 p.p.m. vanadium. The combustion gas was circulated through the furnace via a gas tube which was heated to 200° C (above the dew point for sulphur acid).

The creep furnace was heated by infrared lamps. The furnace was attached to a data track which allowed the programming of any temperature cycle, limited by the heat capacity of the specimen. A thermocouple attached to the specimen registered its surface temperature during each cycle. In order to detect the temperature response of the specimen interior, the centre temperature of one specimen was measured by means of a thermocouple mounted in a hole drilled along the specimen axis. The centre and the surface temperatures were then recorded over several cycles, both during the initial test phase and after 700 h of creep/corrosion. During this period there was negligible change in the shape of the temperature against time curve. A representative cycle from the end of the test is shown in Fig. 1. It is seen that the temperature response is quite similar in the bulk and at the surface, and that during a 12 min cycle, the centre temperature never completely reaches the maximum surface temperature. The difference between the maximum temperatures at the surface and in the bulk is 6 degrees.

The loading system of the creep furnace did not compensate for the reduction in specimen diameter, so only constant load tests were done. The instantaneous creep strain was registered via the movement of the lever arm.

2.2. Specimen preparation

Hot rolled bars (25 mm diameter) of the materials Nickel 201 and Inconel 600 were provided by Henry Wiggin & Co. Ltd, Hereford, England. The nominal composition of the alloys is given in Table I. Both alloys were delivered with a grain size of 15 μm.

Some of the material was heat treated before the test. The annealing was done in evacuated quartz ampoules ($\sim 10^{-5}$ torr) which were subsequently water cooled. All pre-heating was performed before the machining of specimens.

Specimens were machined to standard dimensions of 22.5 mm gauge length and 4.53 mm diameter. The total creep strain was measured after the test from markings on the specimen shoulders. Two sets of markings on opposite sides of the specimen were applied to correct for possible bending during the test.

2.3. Specimen examination

Transverse and longitudinal sections of the exposed specimens were analysed in a Reichert McF2 light

TABLE I Composition of Nickel 201 and Inconel 600 (wt %)

Alloy	Ni	Co	C	Mn	Fe	S	Si	Cu	Cr	Ti
Nickel 201	99.2	0.1	0.020	0.2	0.3	0.010	< 0.1	< 0.1		
Inconel 600	Bal.	0.1	0.15	0.1	8.9	0.015	0.2	0.3	16.5	0.3

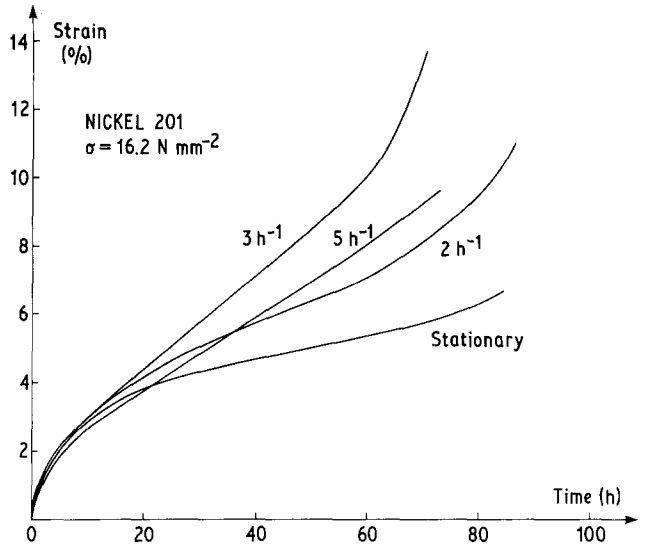

Figure 2 Creep of Nickel 201 at 16.2 N mm^{-2} under stationary (900° C) and variable temperature conditions. The cyclic creep curves are identified by numbers giving the frequency of temperature drops from the holding temperature 900° C.

microscope. The composition of the corrosion products was determined by means of an electron microprobe analyser.

3. Experimental results

The thermal cycling experiments were performed by introducing periodic temperature drops from a fixed holding temperature of 900° C. During each drop, the temperature fell to about 510° C in 3 min, after which the temperature was immediately raised to 900° C over the next 3 min. The cycle frequency was varied by varying the duration of the holding time between each temperature drop. Different holding times were chosen, i.e. 30, 15, 6 and 0 min, giving frequencies of about 2, 3, 5 and 10 cycles per hour. The frequency was kept constant throughout each experiment. The experimental results were compared with creep data obtained at stationary temperature at corresponding stress levels (equivalent to a frequency of zero). All tests were done in combustion gas.

TABLE II Experimental conditions and results for stationary and cyclic creep tests on Nickel 201.

Stress (N mm^{-2})	Frequency (h^{-1})	t_R (h)	$t_{900°C}$ (h)	Elongation (%)	No. of cycles
16.2	0	84	84	6.7	0
	2	86	72	11.0	175
	~3	71	51	13.7	206
	5	74	37	9.6	307

t_R = total rupture time; $t_{900°C}$ = time spent at 900° C prior to rupture.

3.1. Nickel 201

To avoid grain growth during the tests Nickel 201 was pre-annealed at 1100° C for 30 min. The treatment resulted in a grain size of 200 μm. In this condition the alloy was tested at the frequencies 0, 2, 3 and 5 h^{-1} at a stress of 16.2 N mm^{-2}. The creep curves obtained under both variable and stable temperature are given in Fig. 2. All specimens were tested to rupture. As can be seen, the creep rates at variable temperature are larger than under stationary conditions, and there seems to be a tendency for the *total* rupture time to be reduced when the frequency is increased, Table II. However, a more interesting comparison is the time spent at the holding temperature before rupture as a function of frequency. These times are given in Table II, and in Fig. 3 they are represented graphically. It is seen that five temperature drops per hour reduce the time spent at the holding tem-

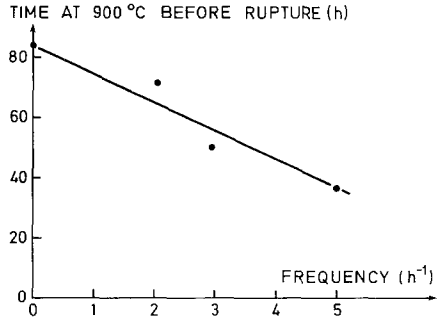

Figure 3 Cyclic creep of Nickel 201. Time at the holding temperature 900° C before rupture as a function of frequency of temperature drops.

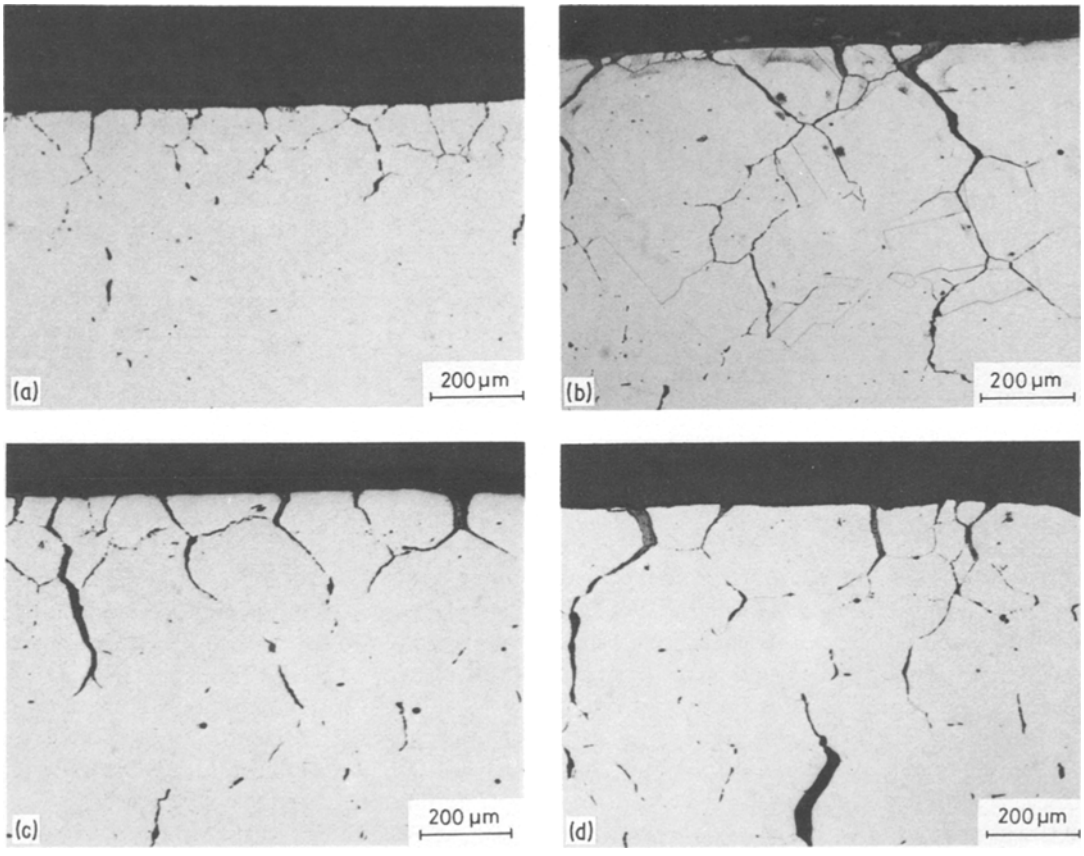

Figure 4 Surface crack propagation in Nickel 201 creep tested at 16.2 N mm^{-2} under stable (900° C) and variable temperature conditions. All micrographs are taken 1 cm away from the fracture surface. (a) Stationary creep: (b) cyclic creep, 2 h^{-1}; (c) cyclic creep, 3 h^{-1}; (d) cyclic creep, 5 h^{-1}.

perature by more than 50%. The effect increases with increasing frequency.

The rupture elongation is also given in Table II, and it is seen to be larger at cyclic than at stable temperature. The reduction in ductility associated with the frequency increase from 3 to 5 h^{-1} is probably accidental. From Fig. 2 it is seen that the 5 h^{-1} specimen has behaved abnormally as rupture has occurred almost without a preceding tertiary creep stage.

Metallographic longitudinal section micrographs, taken 1 cm from the fracture surface, are shown in Figs. 4a to d, the frequency increasing from (a) to (d). The micrographs show that a high density of deep inter-granular cracks has developed from the surface of the cycled specimens, while only relatively shallow subsurface cracks can be detected in the specimen tested at constant temperature. Fig. 5 contains further examples of cracks in the specimen cycled at a frequency of 2 h^{-1}. Fig. 5a illustrates that such cracks develop in regions which otherwise are free from creep cavitation. Fig. 5b is a magnification showing cracks in the NiO surface scale as well as oxidation attacks along the grain boundaries.

3.2. Inconel 600

Inconel 600 was tested in both as-received (small-grained) and in annealed conditions. To obtain a coarse grain structure and a dense intra-granular carbide dispersion which would remain stable during the tests, the alloy was homogenized at 1200° C for 21 h and precipitate-annealed at 900° C for 96 h. The grain size obtained after the solution treatment was about 200 μm.

The test conditions and the experimental results for Inconel 600 are given in Table III and by the creep curves in Figs. 6 and 7. Both the as-received and the annealed material were tested at three different loads. For both materials the two lowest loads gave very similar relationships between the stationary and cyclic creep curves. The medium

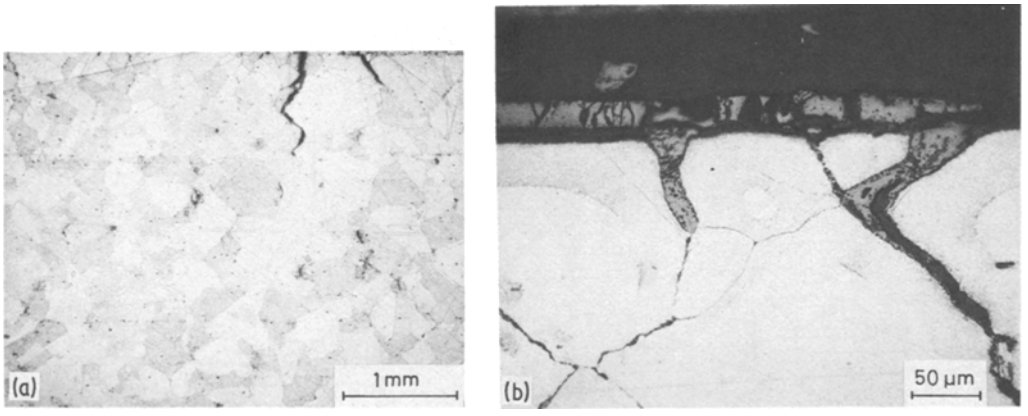

Figure 5 Formation of surface cracks in Nickel 201 cyclic creep tested at 16.2 N mm^{-2} and a temperature drop frequency of 2 h^{-1}. (a) Surface cracks in a region free from bulk cavitation. (b) High density of cracks in the surface oxide scale.

loads are therefore omitted from Figs. 6 and 7. At each load, one specimen was tested at constant temperature and one or two specimens at variable temperature. With two exceptions, the cyclic experiments were run at a frequency of 5 h^{-1}. Both exceptions concern the as-received material. At the highest stress level, 20 N mm^{-2}, a frequency of 2 h^{-1} was used, and at 8.9 N mm^{-2} an additional test was run at 10 h^{-1}. In the latter case there was no holding time at 900° C, and the specimen did not rupture during the test time.

The temperature variations seemed to have a smaller influence on Inconel 600 than on Nickel 201. However, the effect of the cycles was stronger for the annealed than for the as-received variant of alloy 600, and the effect seemed to increase with decreasing load. Thus, at the two lowest stresses the annealed material crept faster during cyclic than during stationary creep (see Fig. 7b for the lowest stress). In all other cases a higher absolute creep rate was registered during stationary than during cyclic creep, as indicated in Figs. 6 and 7a. These facts seem to reflect an increasing sensitivity to temperature variation with increasing grain size and decreasing stress.

A reduction in the absolute rupture time, t_R, upon cycling was observed only for the annealed material tested at the lowest load. Otherwise, the rupture time was shortest during stationary creep. However, except for high loads, cycling had a pronounced effect on the fraction of the lifetime spent at the holding temperature (Table III). The effect was strongest for the annealed, coarse-grained, material for which the time spent at 900° C was reduced by a factor of maximum 2.5 upon cycling.

As for Nickel 201, the temperature cycles generally resulted in an increase in the rupture elongation. An interesting fact to note is that the ductility increased with decreasing load for the as-received material, while the opposite was true for the annealed material.

TABLE III Experimental conditions and results for stationary and cyclic creep tests on Inconel 600.

Material	Stationary creep			Cyclic creep				
	Stress (N mm^{-2})	t_R (h)	Elongation (%)	Frequency (h^{-1})	t_R (h)	$t_{900°C}$ (h)	Elongation (%)	No. of cycles
As-received	20.0	37	59	~2	49	40	59	92
	12.0	177	54	5	235	118	86	1175
	8.9	727	128	5	864	432	154	4318
				10	1995*	0	69*	19 950*
Annealed	40.0	11.3	40	5	25	12.5	45	127
	30.0	77	23	5	99	49.5	37	314
	24.0	210	18	5	176	88	23	880

* = termination (specimen did not rupture); t_R = total rupture time; $t_{900°C}$ = time spent at 900° C prior to rupture.

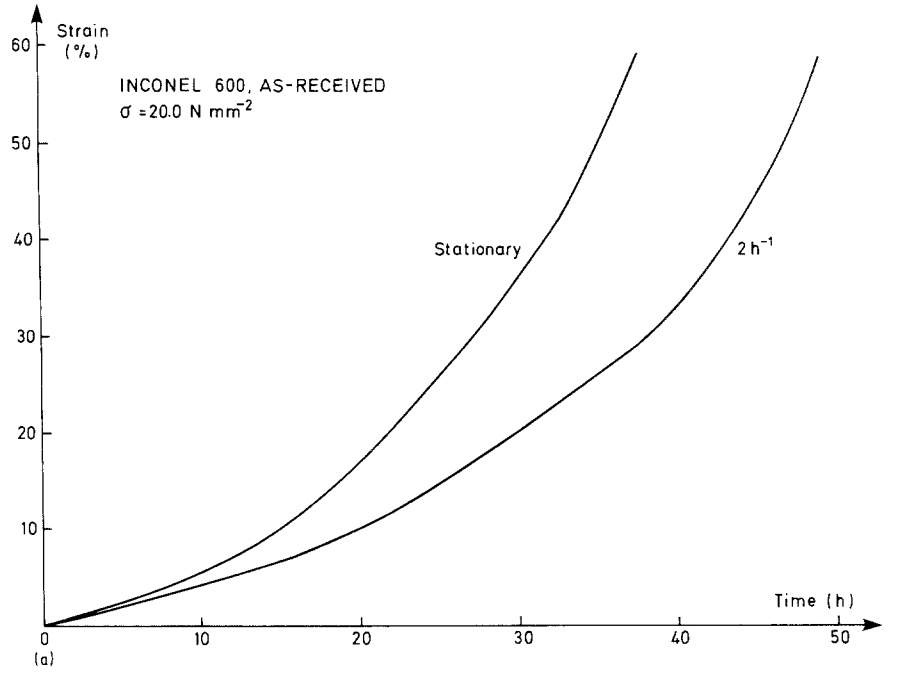

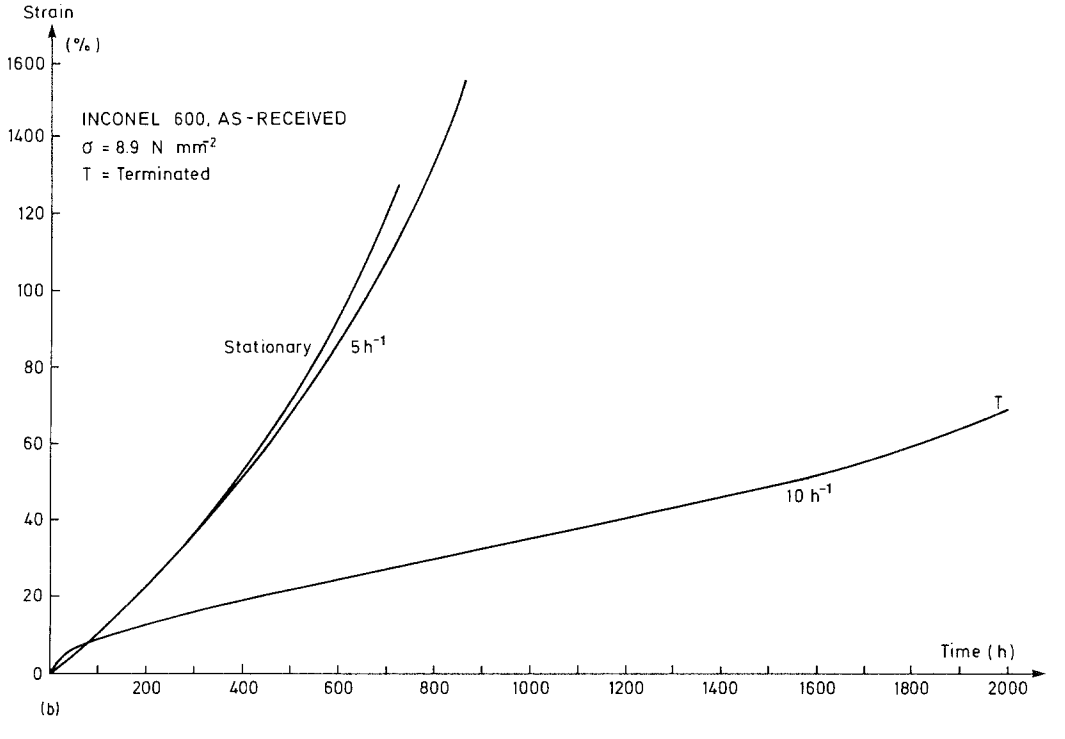

Figure 6 Creep of as-received Inconel 600 under stationary (900° C) and variable temperature conditions, i.e., periodic temperature drops of 390° from the holding temperature 900° C. (a) Stress 20.0 N mm^{-2}, drop frequency 2 h^{-1}. (b) Stress 8.9 N mm^{-2}, drop frequencies 5 h^{-1} and 10 h^{-1}.

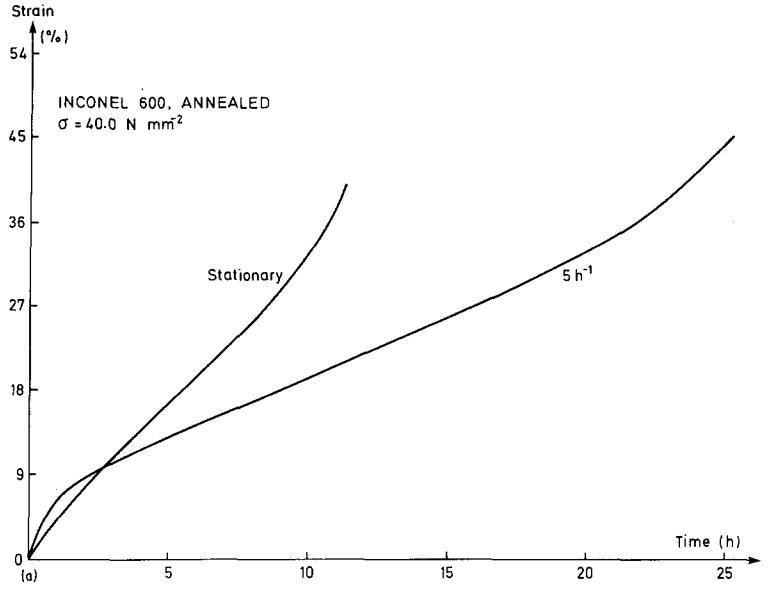

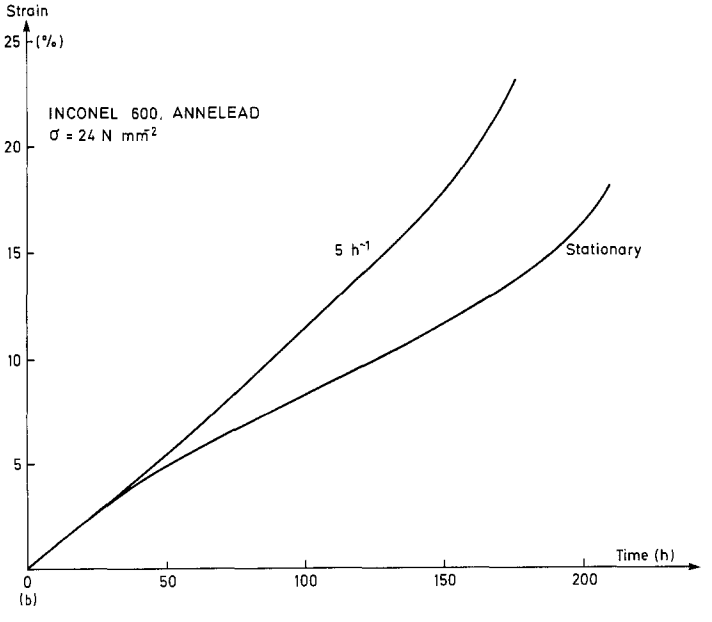

Figure 7 Creep of annealed Inconel 600 under stationary (900° C) and variable temperature conditions, i.e., periodic temperature drops of 390° from the holding temperature 900° C. (a) Stress 40.0 N mm^{-2}, drop frequency 5 h^{-1}. (b) Stress 24.0 N mm^{-2}, drop frequency 5 h^{-1}.

In all the as-received specimens a high density of bulk and surface microcracks had developed in a zone behind the rupture surface. This zone was, however, far deeper in the cycled than in the corresponding stationary creep specimens. The depth of the zone increased with decreasing load. Behind the zones, the density of bulk microcracks decreased rapidly. A high density of oxide-filled surface cracks was, however, observed throughout the gauge length of both the cyclic and the stationary creep specimens, see Fig. 8, which are taken about 1 cm away from the fracture surface. Fig. 8a is from the specimen tested at stable temperature, and Fig. 8b from the cycled specimen. The cracking is clearly most severe in the cycled specimen. The surface cracks were absent on the shoulders of all the Inconel 600 specimens. Obviously, these cracks are therefore purely creep initiated cracks. Occasionally, nitride particles were observed by the cracks.

Micrographs from the pre-annealed, large-grained, Inconel 600 are shown in Fig. 9. The micrographs are taken about 1.5 cm from the fracture surface, (a) from the stationary creep specimen and (b) from the cycled specimen. Close to the rupture surface there was a relatively high

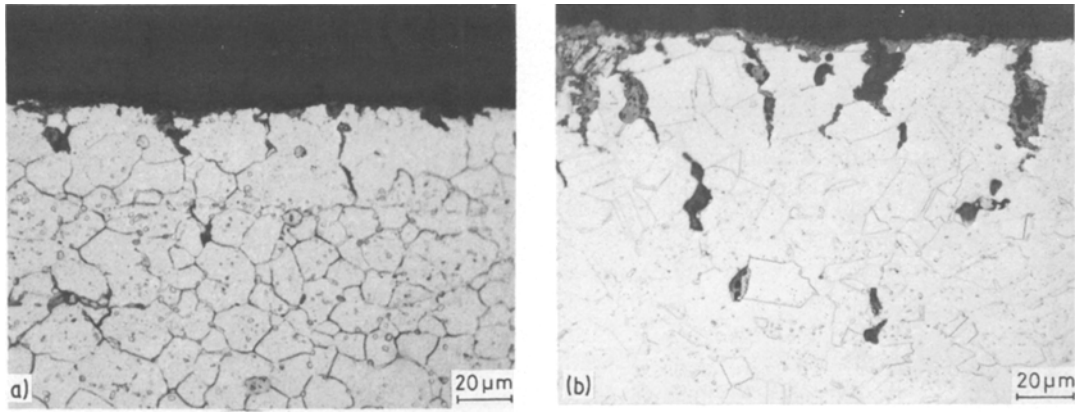

Figure 8 Crack formation in as-received Inconel 600 creep tested at 20.0 N mm^{-2} under stable (900° C) and variable temperature conditions, i.e., cyclic temperature drops from 900° C at a frequency of 2 h^{-2}. (a) Stationary creep, 1 cm behind fracture surface. (b) Cyclic creep, 1 cm behind fracture surface.

density of surface and bulk cracks. Behind the fracture region, however, the majority of cracks had nucleated at the surface, as shown in Fig. 9. Behind the fracture region the surface cracks were also much longer and wider than the bulk cracks. These observations show that surface cracking has been the dominant cracking mode which, consequently, has proved to be the case for all three materials under investigation.

4. Discussion

4.1. Numerical considerations

For both alloys, the time spent at 900° C prior to rupture was generally shorter when the temperature was cycled than when it was kept constant. Exceptions occurred only for the two Inconel 600 variants at their highest respective loads.

However, in comparing the times spent at holding temperature prior to rupture, the periods spent at lower temperatures during the temperature drops are overlooked. It is therefore more correct to introduce a time parameter which includes these periods. Such a parameter can be found by inspecting the expression for accumulated strain in the secondary creep range,

$$\epsilon = A\sigma^n \int_0^t \exp\left[-Q/kT(t)\right] dt, \qquad (1)$$

where

A = constant

σ = applied stress

n = stress exponent

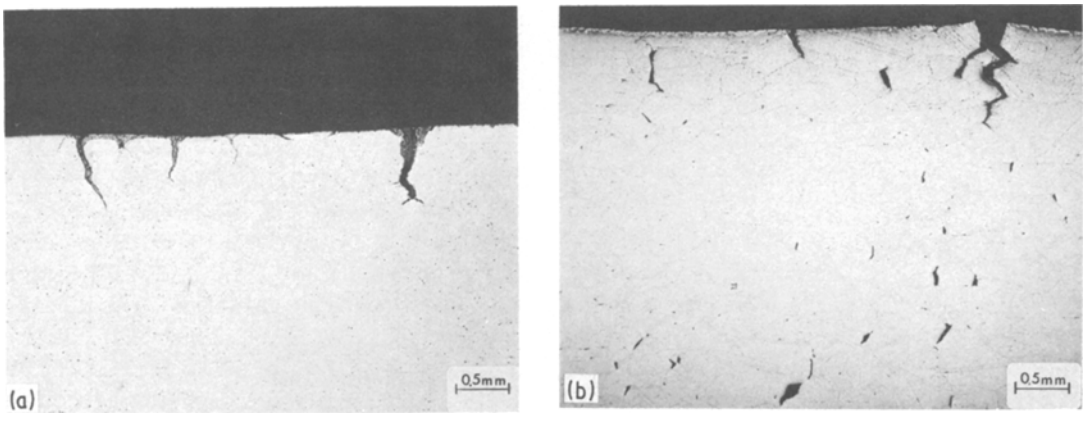

Figure 9 Crack formation in annealed Inconel 600 tested at 30 N mm^{-2} under stable (900° C) and variable temperature conditions, i.e., cyclic temperature drops from 900° C at a frequency of 5 h^{-1}. (a) Stationary creep, 1.5 cm behind fracture surface. (b) Cyclic creep, 1.5 cm behind fracture surface.

t = time

Q = activation energy

k = Boltzmann's constant

$T(t)$ = temperature as a function of time.

Assuming that no change in creep mechanism occurs during cooling to 510°C, Equation 1 should hold for both the stationary and the cyclic creep experiments. The integral in Equation 1 represents the parameter we are seeking because, for equal values of this integral equal values of accumulated strain are theoretically obtained during the two types of creep experiments. This parameter was first introduced by Dorn [2] who found that the creep strain is a function of temperature, stress and compensated time:

$$\theta = \int_0^t \exp\left[-Q/kT(t)\right] \mathrm{d}t.$$

To obtain a parameter with more easily recognizable values, we multiply θ by $\exp\left[Q/kT_{\max}\right]$, where $T_{\max}$ is the holding temperature. In doing this, we have to divide A in Equation 1 by the same factor, to obtain

$$\epsilon = A'\sigma^n \left\{\exp\left[Q/kT_{\max}\right] \int_0^t \exp\left[-Q/kT(t)\right] \mathrm{d}t\right\}$$

$$= A'\sigma^n \Theta, \qquad (2)$$

where $A' = A \exp\left[-Q/kT_{\max}\right]$. The parameter

$$\Theta = \exp\left[Q/kT_{\max}\right] \int_0^t \exp\left[-Q/kT(t)\right] \mathrm{d}t$$

$$= \exp\left[Q/kT_{\max}\right] \theta$$

reduces to t for the stationary creep case. For creep under variable temperature Θ represents an "effective time", which is the time the specimen has to spend at $T_{\max}$ during stationary creep to obtain the same strain as after a time t at variable temperature.

To calculate the parameter Θ we must obtain an expression for the temperature function $T(t)$. For stationary creep it is equal to the holding temperature $T_{\max}$. For simplicity, we assume the sudden temperature changes during the cyclic experiments to be linear with time, both during the falling and the rising portion. This is a reasonable approximation since the actual temperature curve during the temperature fall lies under the linear curve by approximately the same amount as it lies above the linear curve during the temperature rise. We therefore obtain the following expressions for $T(t)$ (the symbols are defined in Fig. 1):

Stationary creep:	$T = T_{\max}$	for all t
Cyclic creep:	$T = T_{\max}$	at holding temperature
	$T = T_{\max} - \dfrac{T_{\max} - T_{\min}}{t_f} \Delta t_f$	during temperature fall
	$T = T_{\min} + \dfrac{T_{\max} - T_{\min}}{t_r} \Delta t_r$	during temperature rise

With the above expressions for $T(t)$ the integral Θ was calculated by means of a computer by subdividing the periods of changing temperature into intervals of one degree K. The creep activation energy Q was set equal to the activation energy for self-diffusion. This is correct for the nearly pure nickel alloy, but need not always be the case for metals high on alloying elements. However, since Q enters the expression for Θ only during the temperature drops [is cancelled for $T(t) = T_{\max}$], a wrong Q value will only affect the effective time contributions from these drops. Due to the low temperatures involved these contributions will in any case be relatively small, and the total error should not therefore be large. The activation energy for nickel diffusion in Nickel 201 was set equal to 2.95 eV [3]. The corresponding activation energy for Inconel 600 was estimated at 3.0 eV on the basis of diffusion data for Ni–20% Cr [4] and Ni–10% Cr [5]. The creep curves of Figs. 2, 6 and 7 were then redrawn with Θ as time parameter, as shown in Figs. 10 to 12. Again the Inconel 600 curves for the medium loads are omitted from the presentation. These curves are qualitatively very much like those for the lowest loads. If creep under cyclic temperature had satisfied Equation 2, the dashed graphs for cyclic creep in Figs. 10 to 12 would have coincided with the solid graphs for stationary creep. However, in most cases the cyclic

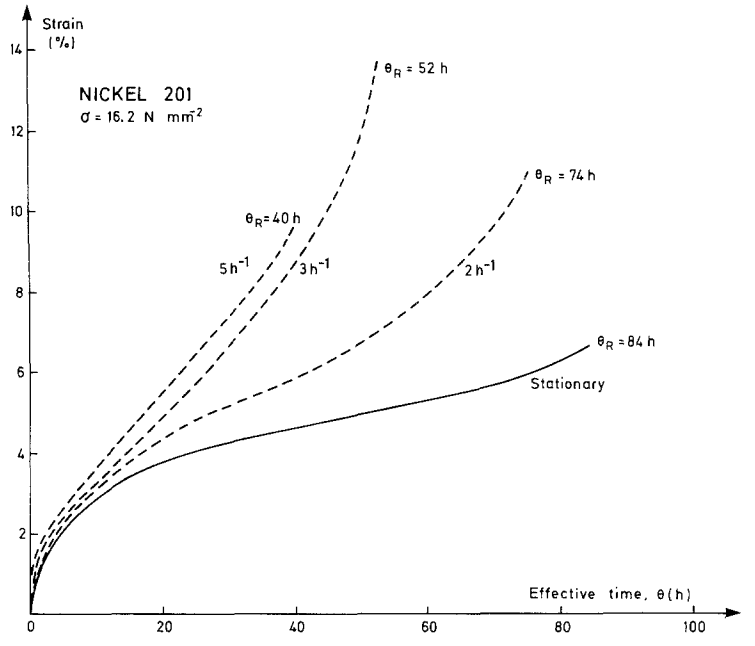

Figure 10 The Nickel 201 creep curves of Fig. 2 redrawn with the effective time Θ as abscissa.

creep curves are positioned well above the corresponding normal creep curves. In these cases creep under varying temperature is therefore effectively faster than stationary creep ("effectively" refers to the effective time Θ). For all three materials the increase in compensated creep rate increases with increasing frequency of temperature drops. The figure by the end point of each graph is the value of the effective rupture time Θ_R which, in the most extreme cases, is seen to be reduced by 52 and 54%, respectively, for the two alloys.

No increase in effective creep rate upon cycling occurred for the two Inconel 600 variants tested at their highest respective loads, Figs. 11a and 12a. The deviation between the graphs for stationary and effective cyclic creep in these cases is probably caused by material scatter. For high loads it thus seems that the temperature drops have little or no influence on the creep behaviour.

By comparing the data in Figs. 10 to 12 with those in Tables II and III we see that the Θ_R-values are only slightly larger than $t_{900^\circ C}$, the accumulated times spent at 900° C during the cyclic experiments. The reason for this is, of course, that the creep rate falls dramatically with temperature. Thus, one temperature drop of 6 min (3 min down and 3 min up) corresponds to 35 sec at the holding temperature. A high frequency of temperature drops is therefore needed for the lower temperatures to contribute noticeably to the theoretical creep strain. This fact is reflected in the increasing difference between Θ_R and $t_{900^\circ C}$ with increasing frequency.

4.2. Metallurgical considerations

The physical reason for the observed effects of the temperature variations is probably connected to stresses set up in the specimens as a consequence of thermal volume changes. We will first recapitulate a theory previously advanced by Brophy and Furman [6] for increased creep rate due to interior stresses, and subsequently bring forward a model for reduced creep strength based on enhanced surface cracking due to oxidation. Finally, the possibility for explaining the effect of the temperature cycles by increased interior cracking will be considered.

4.2.1. Interior thermal stresses

A possible origin of the reduced high temperature creep life of the cycled specimens is bulk thermal stresses introduced during cooling to the lowest temperature of the cycles. In one of the early papers on non-steady creep, Brophy and Furman [6] observed that an increase in strain rate occurred when stainless steel was subjected to a temperature fall from a high creep temperature. This phenomenon was attributed to constrictive forces exerted by the outer layer on the core as a result of a temperature gradient set up during the rapid cooling. A proof of this conclusion was offered by experiments on thin-walled cylinders which did

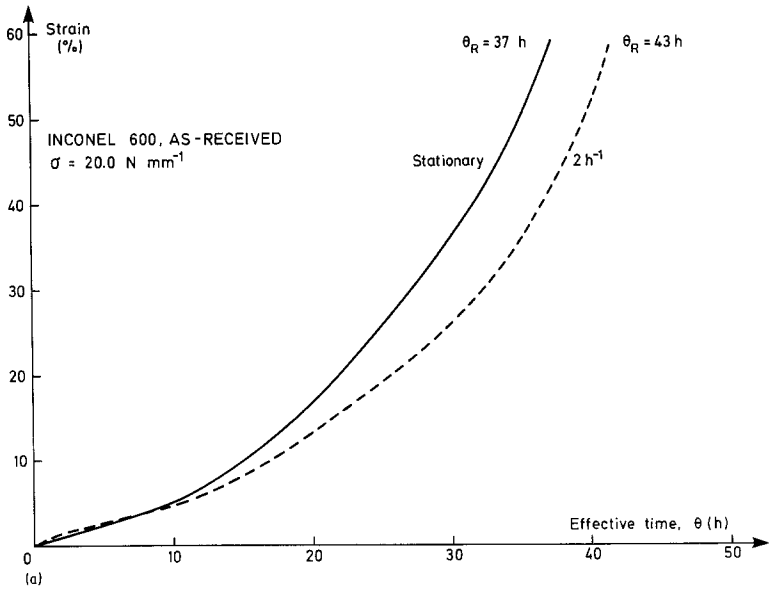

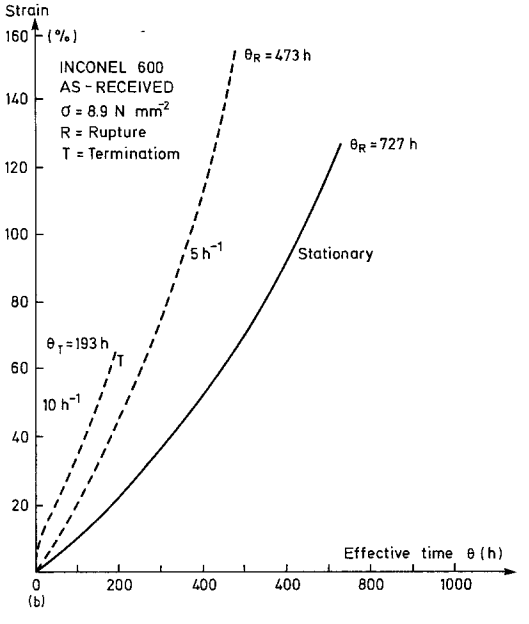

Figure 11 The creep curves of as-received Inconel 600 redrawn with the effective time Θ as abscissa. (a) The curves of Fig. 6a. (b) The curves of Fig. 6b.

not exhibit increased strain during thermal stresses due to the lack of constraint. It was also reported that the effects were absent in bar stock if the temperature was changed very slowly. The Brophy–Furman model may provide an explanation of the increased creep rate during temperature cycling observed in this work, and hence, also of the reduced time to rupture. A possible test of the validity of the theory for the present case would be, either to do careful extensiometer readings during the cooling part of the cycles, or to perform experiments on thin-walled cylinders. The Brophy–Furman model will be discussed further in the light of the present results in Section 4.2.4.

4.2.2. Surface cracking due to oxidation

In the present investigation the effect of the temperature cycling did strongly depend on the grain size of the material. This fact indicates that increased crack growth may be an alternative source of reduced creep resistance under variable temperature. Crack formation at the surface appeared to be the dominating cracking mode for both Nickel 201 and Inconel 600, Figs. 4, 5, 8 and 9. This phenomenon is probably associated with grain boundary oxidation and, for Nickel 201, perhaps also with the formation of a thick surface oxide layer.

As described in [1], creep of the two alloys resulted in a strong increase in the grain boundary corrosion attacks. The oxidation products were of type NiO for Nickel 201 and mainly of type Cr_2O_3 for Inconel 600. Oxides have generally a smaller coefficient of thermal expansion than metals. During temperature cycling, the grain boundary oxides experience therefore only minor volume changes compared to the surrounding metal which contracts and expands. An estimate of the thermal stresses set up in front of an oxide tip because of these pulsations is given below.

Consider the grain boundary oxide in Fig. 13a at the maximum temperature 900° C. The interface segment AB is perpendicular to the grain boundary which is drawn with a thick line. The oxide is assumed to be formed mainly at the

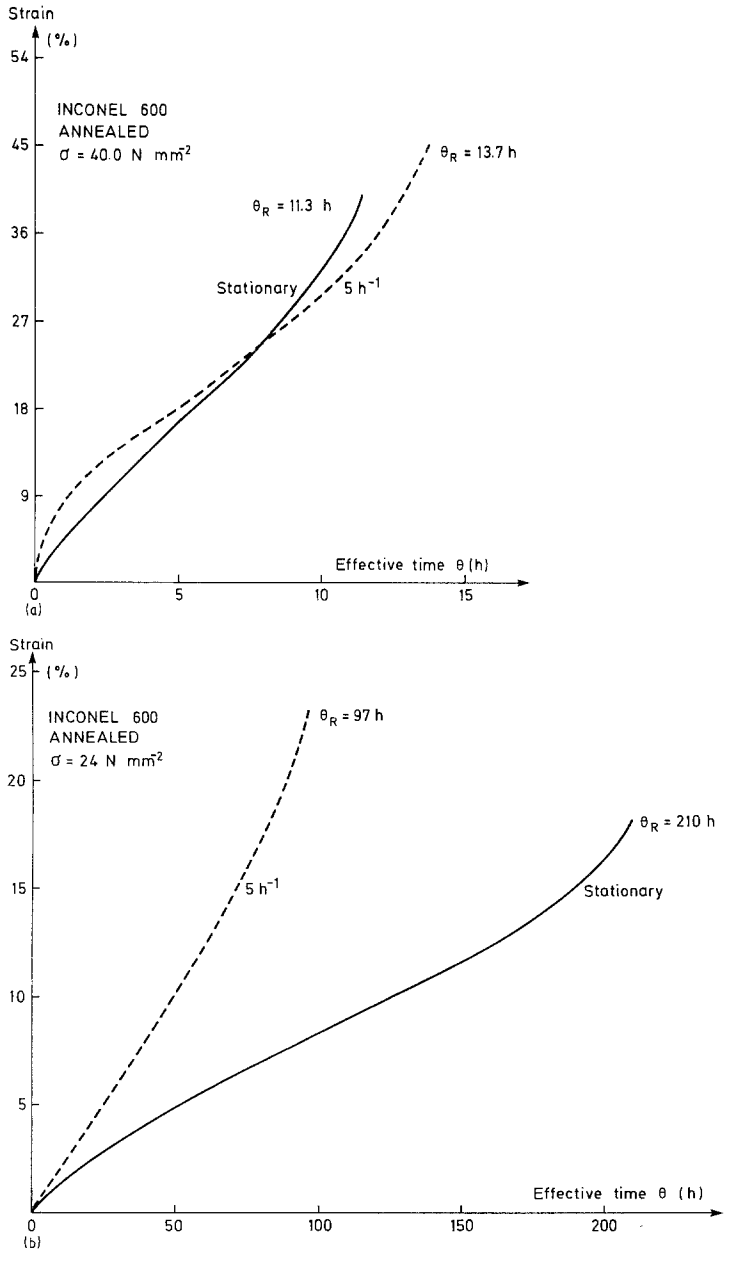

Figure 12 The creep curves of annealed Inconel 600 redrawn with the effective time Θ as abscissa. (a) The curves of Fig. 7a. (b) The curves of Fig. 7b.

holding temperature 900° C, and for the sake of illustrating the effect of the temperature cycles alone it is assumed that the oxide causes no stresses in the matrix at 900° C. The crystal planes parallel to the grain boundary are therefore drawn as straight lines on either side of the boundary. (The incorporation of matrix strains due to a volume increase upon oxidation would have increased the stresses calculated below.) The temperature then drops to its minimum value of 510° C, and the oxide and the metal shrink in volume. However, because the thermal contraction is stronger in the metal than in the oxide, tensile stresses arise in the metal in front of the oxide tip. This is indicated by the curved crystal planes in Fig. 13b. Assuming that no strain is set up in the oxide, the matrix strain $\epsilon_{m/o}$ in the AB direction in front of the oxide tip corresponds to the difference in thermal contraction between the two phases. Thus:

$$\epsilon_{m/o} = (\alpha_m - \alpha_o)\,\Delta T,$$

where α is the linear coefficient of thermal expansion, the subscripts m and o identify the metal

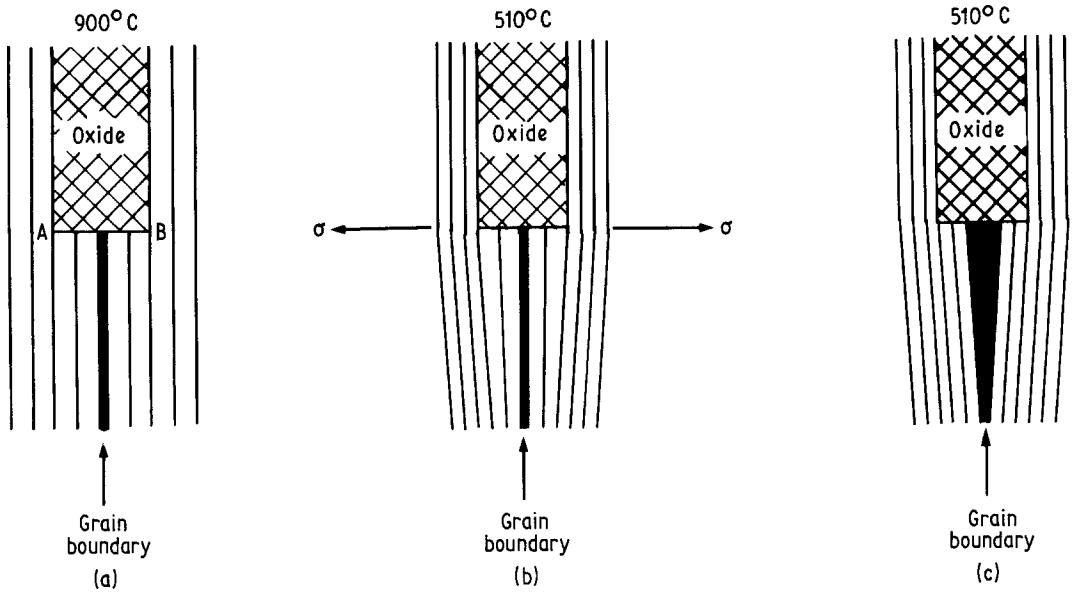

Figure 13 A schematic illustration of the nucleation of a microcrack in front of a grain boundary oxide during temperature cycling between 900° C and 510° C. (a) The oxide is assumed to be formed at 900° C and is assumed to cause no elastic strain at this temperature. (b) Cooling to 510° C causes strains in front of the oxide tip due to the contraction of the nickel matrix. (c) The strains nucleate a grain boundary microcrack in front of the oxide.

and the oxide phase, and ΔT is the temperature difference between the maximum and the minimum temperature of each cycle (390 K). The corresponding thermal tensile stress in the AB direction is then

$$\sigma_{m/o} = \epsilon_{m/o} E = (\alpha_m - \alpha_o)\Delta T E,$$

where E is the Young's modulus of elasticity of the metal. (This is a slight over-estimate of the stress since it will be reduced by compression strains in the oxide. Due to high E values in oxides these strains are ignored, however.)

Values for the thermal expansion coefficients and the modulus of elasticity of the involved phases are given in Table IV. Assuming that the difference in α between Nickel 201 and NiO is the same in the temperature range 510 to 900° C as in the range 300 to 800° C (Table IV), we obtain

$$\sigma_{201/NiO} = 228\,N\,mm^{-2}.$$

Correspondingly, if we assume that α for Cr_2O_3 has the same value in the temperature range 510 to 900° C as in the range 20 to 1400° C, we get

$$\sigma_{600/Cr_2O_3} = 639\,N\,mm^{-2}.$$

The 510° C values of the 0.2% proof stress and the tensile strength are, respectively, 86 $N\,mm^{-2}$ and 244 $N\,mm^{-2}$ for Nickel 201 (annealed [7]), and 198 $N\,mm^{-2}$ and 587 $N\,mm^{-2}$ for Inconel 600 (hot-rolled [7], the value may be larger for annealed material). The calculated stress values in front of the oxide tips are thus much higher than the proof stress of the respective metals and of the same magnitude as the tensile strength. Of course, the actual

TABLE IV Linear coefficients of thermal expansion, α, and Young's modulus of elasticity, E

Phase	$\alpha(10^{-6}\,°C^{-1})$	$E(10^3\,N\,mm^{-2})$	Temperature range (° C)	Reference
Nickel 201	17.2		300–800	[7]*
Nickel 201		189	510	[7]*
NiO	14.0		300–800	[8]
Inconel 600	18.4		510–900	[9]*
Inconel 600		187	510	[9]*
Cr_2O_3	9.6		20–1400	[8]

*Calculated from data in this reference.

values are reduced by material flow since the yield stress is exceeded. However, the important fact is that plastic stress peaks build up in front of the grain boundary oxides during the temperature falls. These stresses probably open microcracks along the weak boundaries in front of the oxides, Fig. 13c. The nucleated microcracks reduce the load-bearing cross-section of the specimen and result in increased creep during the succeeding period(s) at maximum temperature. When the bulk material in front of the crack tip elongates, the crack widens correspondingly. Again it will be filled with oxide which causes further crack growth during the next temperature drop. The whole crack growth sequence is illustrated in Fig. 13. According to this model a grain boundary crack will grow faster at variable temperature than it would have done under stationary temperature conditions, illustrated in Fig. 5 for Nickel 201. This will naturally result in a higher effective creep rate during cyclic than during stationary creep, Figs. 9 to 12. In some cases the effect of the cycles may be strong enough to cause an increase even in the absolute creep rate, as observed in Figs. 2 and 7b and c.

In the foregoing we have only considered grain boundary oxides as the reason for increased surface cracking during cycling. However, the surface oxide scale might be an additional source of increased surface crack formation during cycling. This might especially be the case for Nickel 201 which develops a very thick oxide scale. The temperature cycling probably leads to increased crack formation in the surface scale. When such a crack is formed right outside a grain boundary as in Fig. 5b, it might nucleate a grain boundary crack in the substratum. However, from micrographs like that in Fig. 5b it is difficult to decide which of the two cracks came first, the surface scale crack or the grain boundary crack. Further evidence for grain boundary cracking due to surface scale cracks is therefore difficult to provide.

Of course, the described model does not serve as a complete model for creep crack growth under variable temperature and oxidizing conditions. In the model, we have only described the *additional* effects brought about by the temperature cycles. We have not discussed the origin of surface creep cracks in oxidizing environments, but only taken the existence of such cracks as a basis for explaining the net damaging effect of the temperature cycles. A complete theory must, for instance, take into consideration possible matrix strains due to a volume increase accompanying oxidation, as well as the complex stress field generally existing around a creep crack tip. Some of these effects are discussed in [1].

4.2.3. Interior microcracking

Although surface cracking appears to be the dominant cracking mode, the possibility of increased creep due to enhanced nucleation of interior creep cracks upon temperature cycling must be considered. This might especially be considered to be the case for Inconel 600 where the grain boundaries are decorated by carbides and occasionally by nitrides having diameters up to 5 and 10 μm respectively. Owing to the difference in thermal expansion between these particles and the surrounding matrix, the inclusions will be sources of fluctuating local stresses during the temperature variations. As in the case of the grain boundary oxides, these stresses may nucleate grain boundary microcracks. However, this process will not repeat itself because the nucleated microcracks will not be filled with new material as was the case for the surface cracks. The wedge-like effect of the particles will therefore cease. In accordance with this fact, large microcracks were only occasionally observed to have formed near particles. In fact, there are reasons for believing that the particles have only minor, if any, influence on the increased crack formation during cycling. Firstly, no cracks or only very small cracks had nucleated from the majority of grain boundary particles. Secondly, most of the observed bulk grain boundary microcracks had a typical creep character, i.e. wedge cracks nucleated at triple points. Thirdly, one should seek a model which can explain the effect of the cycles on both the tested materials. Since Nickel 201 contained no grain boundary particles, it is tempting to exclude such particles from the operating mechanism.

Another phenomenon which should be mentioned as a possible cause of increased internal microcracking during cycling is a change in deformation mode towards less dislocation creep with decreasing temperature. This change may lead to increased stress peaks from grain boundary sliding during the temperature drops, and thus to increased microcracking. However, due to the short time intervals spent at lower temperatures this effect is assumed to be small and certainly not the main reason for the increased creep degradation during temperature cycling.

4.2.4. A comparison of the models

It is difficult to decide which of the presented models for accelerated creep during cycling is the most probable one. However, some indications are inherent in the experimental results. First, from the Brophy–Furman model it is difficult to explain that the effects of the cycling vanish at the highest loads. On the contrary, Brophy and Furman detected an increased acceleration in creep rate when the applied stress increased. A reduced effect of the temperature variations with increasing stress is more easily incorporated in a theory based on crack nucleation induced by grain boundary oxides. The creep rate increases strongly with increasing load. For unchanged frequency, a specimen therefore experiences fewer temperature drops per unit of strain at a high than at a low stress. Accordingly, the contribution from the temperature drops on the surface crack growth should decrease with increasing stress, resulting in a decreased sensitivity to temperature drops with increased stress. The observed stress dependency thus points towards a model including surface crack formation.

The strong influence of grain size on the effect of temperature cycling is also contrary to expectations of the Brophy–Furman model. The grain size has no influence on the magnitude of the additional creep stress set up in the specimen during the cooling to lower temperatures. Consequently, the temperature cycling should not discriminate between small- and large-grained specimens. Within our model, however, the dependence on grain size is well accounted for. A crack will naturally grow fast as long as it propagates along the same grain boundary. A transverse boundary in front of the crack tip represents a hindrance for further propagation. Consistent with the present observations, the crack size will therefore generally be larger in a large-grained material than in a small-grained one, and the former material experiences a stronger reduction in load-bearing area than the latter one. Within our model, an increasing acceleration in (effective) creep upon temperature cycling is therefore to be expected to occur with increasing grain size. (Of course, the difference in grain size is also responsible for the much higher rupture elongation observed for as-received than for annealed Inconel 600.)

From a comparison of the creep curves in Fig. 2 and in Fig. 7b ($t_R \sim 100$ h), it appears that the effect of the cycles is somewhat stronger on Nickel 201 than on annealed Inconel 600 despite the identical grain size of these two materials. A reason for this may be found both within the Brophy–Furman theory and within our model including crack formation. In the Brophy–Furman theory, accelerated creep occurs due to constrictive forces exerted by the outer layer on the core as a result of a temperature gradient which is set up during rapid cooling. The thermal conductivity and the thermal expansion coefficients of the two tested alloys are very similar, and the thermal stresses set up during cooling should therefore be equal. For a weak material like Nickel 201 these stresses amount to a higher fraction of the applied creep stress than for Inconel 600. Accordingly, the thermal stress should result in a stronger creep contribution in the former alloy than in the latter one.

However, a model based on increased surface cracking can also explain why the temperature drops have a stronger effect on Nickel 201 than on Inconel 600. As reported in [1], Nickel 201 is subjected to thicker oxide scale formation and deeper corrosion attacks than Inconel 600 in a combustion gas atmosphere. This is probably associated with the type of oxide scale formed on the two alloys. Cr_2O_3, which forms on Inconel 600, has a much tighter structure with respect to diffusion than NiO, which forms on Nickel 201. Cr_2O_3 is therefore the more protective of the two oxides, and corrosion is consequently faster in Nickel 201 than in Inconel 600. In addition, the thick oxide scale on Nickel 201 is highly susceptible to cracking during temperature cycled creep, a circumstance which promotes the grain boundary attacks in this alloy. Of these reasons, the repeated wedge-like effect of the grain boundary oxides will probably more effectively accelerate the growth of surface cracks in Nickel 201 than in Inconel 600. In consequence, Nickel 201 is likely to be more strongly affected by the temperature falls from the holding temperature.

In the light of the arguments given above, the experimental results seem to be more consistent with a model for accelerated creep during temperature cycling based on crack growth than with the Brophy–Furman model. Although some of the results can be explained by the latter theory, it can hardly justify all the observations. As an explanation of the results obtained in this work we are therefore inclined to favour the crack growth mechanism proposed by the present

authors. However, in this model oxidation plays an important role. In other cases where corrosion is less significant, other mechanisms may dominate.

4.2.5. Rupture elongation

Tables II and III show that an increase in rupture elongation accompanies the temperature cycling. This observation can be understood both from the increase in effective stress and from the increase in effective creep rate that it is suggested takes place during cycling. In the first place, a stress increase changes the deformation mode in such a way that more of the creep straining occurs by grain deformation. The accompanying grain boundary migration reduces the stress accumulation set up by the grain boundary sliding, and less internal cavitation occurs. A reduced cavitation with increased stress is reported in a variety of materials, e.g., in Nimonic 80A by Dyson and Rodgers [10].

In the second place, the increased effective creep rate which was observed during cycling may also be responsible for the increased ductility. Several models on creep crack growth include a time dependent growth contribution from diffusion, e.g., [11–14]. Although the contribution from diffusion on creep crack propagation has been disputed by many other authors, for example Pilkington *et al.* [15], a large amount of experimental evidence available in the literature suggests that diffusion is associated with cavity growth. The increase in ductility associated with the temperature cycling in the present work fits in well with a model for creep crack growth including diffusion. Due to the increase in strain rate upon cycling the diffusional contribution to crack growth per strain unit will be less during cycling than during stationary creep. In consequence, the internal cracks will grow more slowly as a function of strain during cyclic than during stationary creep, and the ductility is increased as a result of the temperature variations. From the two explanations given above, we see that the increased ductility in cyclic creep might be explained by a complicated model based on increased surface cracking and reduced internal creep cavitation. The reason why the increased surface cracking does not lower the ductility might be that the surface crack growth rate gradually diminishes as the transport distance for oxygen to the crack tip increases.

4.3. Consequences for the life fraction rule

The results of this work clearly demonstrate that temperature variations may cause creep deformation which is not described by existing mathematical expressions for creep straining and rupture life. As a consequence, utmost care should be shown when using constant temperature data as design data for applications including varying temperature. Parts which are subjected to a high frequency of fast temperature changes may rupture earlier than expected from stationary creep data, or from estimates based on the life fraction rule applied on stationary creep data.

Some authors, for example, Pech and Sedlacek [16], have successfully used the life fraction rule on variable temperature creep by dividing the periods of changing temperature into partial intervals and adding together the life fractions calculated from each interval. In this approach, a possible change in creep mechanism during the temperature fall or rise is accounted for. If a material obeyed stationary creep laws in a condition of changing temperature, a rather exact estimate of creep life should therefore be obtained by the use of this method. However, the results of the present and other work (e.g. [6]) show that a cycling temperature may introduce creep damage which is not present during stable conditions. No mathematical approach involving the application of stable creep results on small subdivisions of creep history can therefore correctly predict creep strain in all situations.

Corrosion seems to have played an important role in the degradation of the creep resistance in this work. In most high temperature applications corrosion has a great influence, and its effect on creep properties must be taken seriously and accounted for in the evaluation of the durability of components in machines and plants. As no current theory is capable of including corrosion and thermal cycles to a satisfactory degree, at present experiments seem to be the only tool which can give reliable data for life estimates under such conditions.

5. Conclusions

Nickel 201 and Inconel 600 have been creep tested in combustion gas at constant temperature (900° C) and at variable temperature, i.e., 900° C interrupted by periodic temperature drops down to 510° C. Alloy 201 was tested in the annealed condition, grain size 200 μm, and alloy 600 both as-

received and annealed, grain sizes 15 and 200 μm respectively.

The temperature cycling was generally found to decrease the creep resistance. For both alloys, the time spent at the holding temperature (900° C) prior to rupture was strongly reduced by the temperature drops. A weighted time parameter which takes account of the contribution to creep deformation made during the lower temperatures of each cycle, has been used to compare the creep straining during stationary and cyclic creep. With regard to this parameter, a strong acceleration in creep straining was measured under variable temperature at all except at the highest stresses.

The degrading effect of the temperature cycles was most pronounced for the annealed materials, which indicates a strong influence from the grain size. The effect of the cycling appeared also to increase with increasing frequency and decreasing load. Thus, at the lowest stress levels, the large-grained version of Inconel 600 experienced a reduction even in *absolute* creep life upon cycling. Nickel 201, which was tested only in a large-grained condition and only at one load, experienced at all frequencies a higher *absolute* creep rate during cyclic than during stationary creep conditions.

Although a model based on accelerated creep due to thermal creep stresses may explain some of the experimental results, it is suggested that thermally enhanced cracking from grain boundary oxides is the main reason for the observed effect of the temperature cycling. The oxides are the result of environmental corrosion attacks, and are assumed to form mainly during the holding periods at high temperature. Generally, oxides have a lower coefficient of thermal expansion than metals, and during cooling an oxide particle acts like a wedge and splits the metal matrix along the grain boundary in front of the oxide tip. Repeated oxidation at the holding temperature and subsequent cracking during the cooling periods will make a grain boundary crack grow faster at variable temperature than it would have done under stationary temperature conditions. The model seems to give a reasonable explanation of why the effect of the temperature cycles seems to increase with grain size, frequency and decreasing load, and also why Nickel 201 is more affected than Inconel 600.

Acknowledgement

The authors are grateful to Svein Ove Olsen who was responsible for the experimental work.

References

1. J. K. SOLBERG and H. THON, *Met. Trans.* **14A** (1983) 1213.
2. J. E. DORN, *J. Mech. Phys. Soc.* **3** (1954) 85.
3. K. MONMA, H. SUTO and H. OIKAWA, *J. Jpn. Inst. Metals* **28** (1964) 188.
4. H. WIGGIN & Co. Ltd., "Physical and Mechanical Properties of Nimonic Alloys", Publication 3270 (Hereford, 1967).
5. MARTIN MARIETTA Corp., "MAR-M Alloy 246" (Martin Metals Division, 1969).
6. G. R. BROPHY and D. E. FURMAN, *Trans. ASM* **30** (1942) 1115.
7. H. WIGGIN & Co. Ltd., "Nickel 200 and 201", Publication 3570 A (Hereford, 1972).
8. G. V. SAMSONOV (ed.), "The Oxide Handbook", translated by C. N. Turton and T. I. Turton (Plenum, New York, 1973) p. 126.
9. H. WIGGIN & Co. Ltd., "Inconel Alloy 600", Publication 3269 (Hereford, 1971).
10. B. F. DYSON and M. J. RODGERS, *J. Mater. Sci.* 8 (1974) 261.
11. V. VITEK, *Acta Metall.* **26** (1978) 1345.
12. W. BEERE and M. V. SPEIGHT, *Met. Sci.* **12** (1978) 593.
13. M. V. SPEIGHT, W. BEERE and G. ROBERTS, *Mater. Sci. Eng.* **36** (1978) 155.
14. J. GITTUS, "Creep, Viscoelasticity and Creep Fracture in Solids" (Applied Science Publishers Ltd., London, 1975) pp. 574 and 588–589.
15. R. PILKINGTON, D. A. MILLER and D. WORSWICK, in "Creep in Structures", IUTAM Symposium, Leicester, UK, 1980, edited by A. R. S. Ponter and D. R. Hayhurst (Springer, Berlin, 1981) pp. 525–541.
16. R. PECH and J. SEDLACEK, in "Symposium on The Physical–Metallurgical Problems and Problems Concerning Applied Mechanics in Manufacture of Large-Capacity Turbosets", Prague, 7–9 September 1967, ([Hrsg.:] Vydala práce pro o.p. Škoda plzeň, 1970) Vol. I, p. 138.

Received 14 April 1983
and accepted 24 January 1984